7.1 Introduction

Sb_2Te_3 is a well-known traditional narrow- gap semiconductors having band gap of 0.26 eV, emerged as a three dimensional topological insulator (TI) with a metallic surface conduction and insulating bulk energy gap. The crystal structure of Sb_2Te_3 consists of repeated groups of (Te^1-Sb-Te^2-Sb-Te^1) type of quintuple layers having thickness ~10Å, often known as the tetradymite- type lattice. Since the spin configuration of the surface state is unique in TIs, many interesting phenomena such as magnetic monopole, novel magnetoelctric quantum states and quantum anomalous Hall Effect (QAHE) have been proposed in ferromagnetic TIs [133-134]. Furthermore, besides these interesting properties in TIs, breaking of time reversal symmetry (TRS) on the surface may open a new way for potential applications. Moreover, not only entering substitutionally or interstitially in the parent materials, van der Waals gaps between the layers are also available for the dopants in TIs. Magnetic dopants can break the time reversal protection of the Dirac point, resulting in a band gap due to the separation in the upper and lower branches of the Dirac cone in TIs. Therefore, TIs having magnetic ordering recently attracted great interest for their promising applications in the emerging field of spintronics and many other novel phenomenon discussed above. Consequently, much effort has been done to prepare topological insulators that exhibit magnetic ordering [111,126,127,135-139]. Kim et al. have reported antiferromagnetic ordering below 7K in Gd substituted Bi_2Se_3 single crystals [135]. Yang et al. have found paramagnetic state in Co doped Sb_2Te_3 nanoplates [136]. Li et al. have observed that the ferromagnetic ordering exists only below curie temperature (T_c) ~10.2K in Bi and Cr doped Sb_2Te_3 [111] whereas paramagnetic state has been found in Fe doped Sb_2Te_3 single crystals [137]. Choi et al. reported ferromagnetic ordering in Mn doped Bi_2Te_3

and Sb_2Te_3 single crystals with T_c ~10K and ~17K respectively [138]. Dyck et al. have reported ferromagnetic state with T_c ~22K in the case of Cr doped Sb_2Te_3 single crystals [126] whereas in the case of $Sb_{2-x}V_xTe_3$, they have also found ferromagnetic ordering, and the highest T_c was below 23K for x=0.03 [127]. Drasar et al. observed maximum value of T_c in the case of V and Cr doped Sb_2Te_3 which was below 24K [139] but magnetic ordering at room temperature (RT) is required for the spin based applications. To prepare TIs showing magnetic ordering at room temperature is a challenge now-a-days. In this chapter, we have investigated the structural, surface morphology, chemical analysis and magnetic properties of Co doped Sb_2Te_3 showing room temperature antiferromagnetic ordering with transition temperature above 300K, which may be important for spintronics devices, quantum computing, multifunctional electromagnetic application and disc reading heads.

7.2 Results and Discussion

7.2.1 X-Ray Diffraction Analysis

Room temperature X-ray diffraction (XRD) pattern of $Sb_{2-x}Co_xTe_3$ (x=0, 0.02, 0.06, 0.10) samples have been shown in Fig. 7.1. The XRD peaks were exclusively labeled with the indices (00L) showing the single crystal nature of the as prepared samples. All the XRD peaks were indexed using the standard JCPDS file for Sb_2Te_3 (JCPDS#71-0393) with rhombohedral structure. It is obvious from the XRD patterns that the Co doping does not lead to the presence of any extra peaks indicating the Co doped Sb_2Te_3 retains the rhombohedral crystal structure belonging to the space group $\boldsymbol{D_{3d}^5}$ (R-3m). The Full Width Half Maxima (FWHM) of the (003) peak for the x=0.10 was as small as 0.104^0 which indicates the prepared samples have excellent single crystallinity in long range even at highest doping

concentration of Co. Around $2\theta=54^0$ and 64^0, a small splitting due to the CuK_β radiation is observed. For the determination of lattice

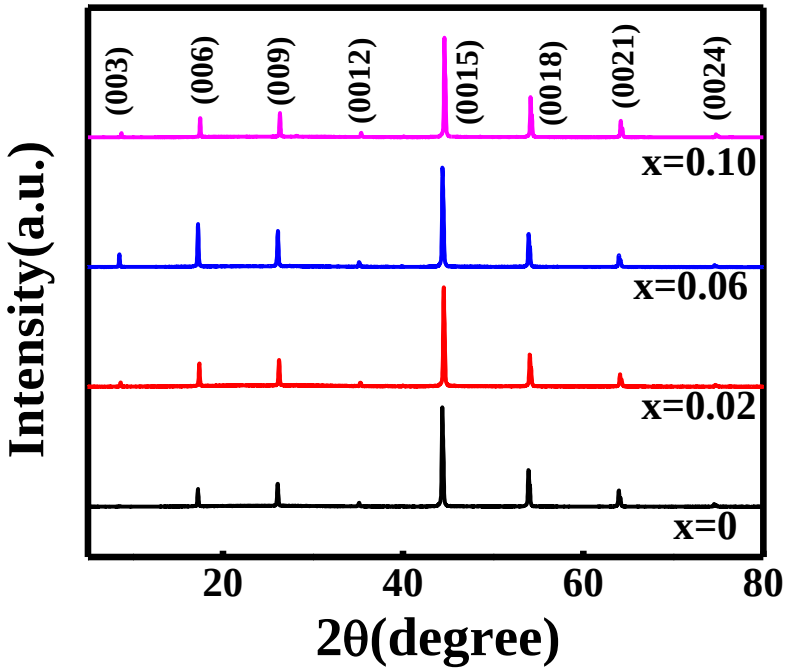

Fig.7.1 X-ray diffraction (XRD) pattern of $Sb_{2-x}Co_xTe_3$ (x=0, 0.02, 0.06, 0.10) single crystals.

parameters (a and c) and the cell volume (V), we have carried out the XRD measurement of the samples in powder form and analyzed it by Le Bail refinement using the Full-Prof suit toolbar which is shown in fig. 7.2. The determined α, β and γ values from Le Bail refinement were 90˚, 90˚ and 120˚ for all of the samples. The FWHM value corresponding to (003) peak has been determined using Gaussian peak fit for the entire samples. The obtained lattice parameters (a, c), interplaner spacing d, FWHM and cell volume (V) are shown in Table-7.1. Change in lattice parameters, FWHM and cell volume support the doping of Co at Sb site. Lattice plane spacing d was increasing with the doping concentration of Co. For the sample x=0.02, the c parameters was less than the undoped sample (x=0), which was found due to

the lower ionic radius of Co than the Sb but with further increase of doping concentration, c parameter was increasing which might be due to the charge repulsive force between the same type of Co ions.

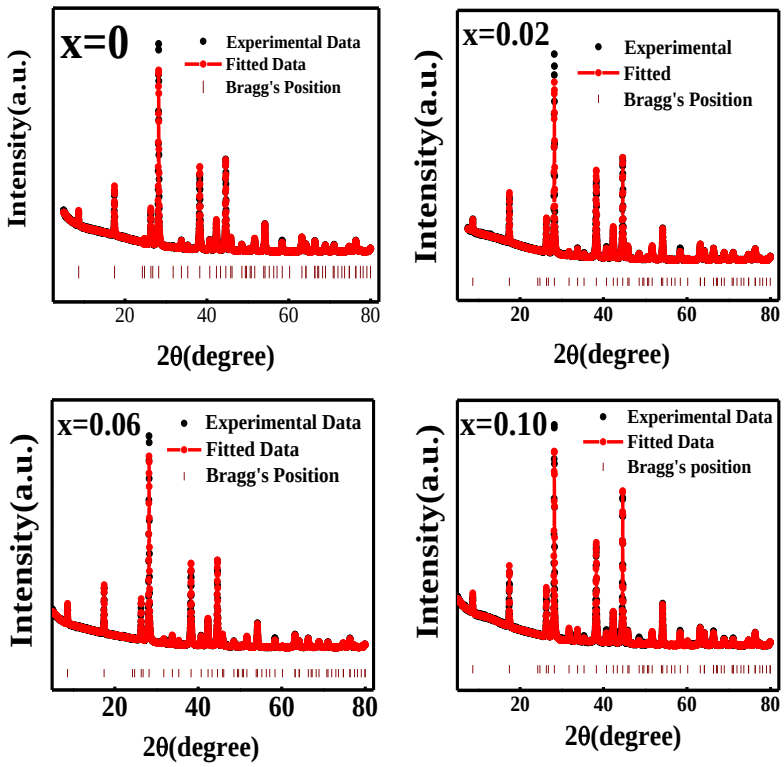

Fig.7.2. Le Bail refinement of the XRD pattern for the samples (x=0, 0.02, 0.06, 0.10).

Table7.1. Different parameters obtained from Le-bail refinement of the samples (x=0, 0.02, 0.06, 0.10).

x	a=b(Å)	c(Å)	d(Å)	FWHM(˚)	V (Å^3)
0	4.2648(0)	30.4381(0)	2.0292(0)	0.1573(5)	479.4529
0.02	4.2655(4)	30.4378(9)	2.0291(9)	0.1268(2)	479.6165
0.06	4.2654(3)	30.4379(6)	2.0291(5)	0.1268(9)	479.5931
0.10	4.2659(2)	30.4448(0)	2.0296(5)	0.1044(4)	479.8106

7.2.2 Elemental and Surface analysis

In order to further confirmation of the presence of Cobalt in doped Sb_2Te_3 single crystals, elemental analysis has been also done using EDX. The performed EDX has been presented in Fig. 7.3(a, b) for x=0 and 0.10 samples respectively. It was obvious from the EDX data that the

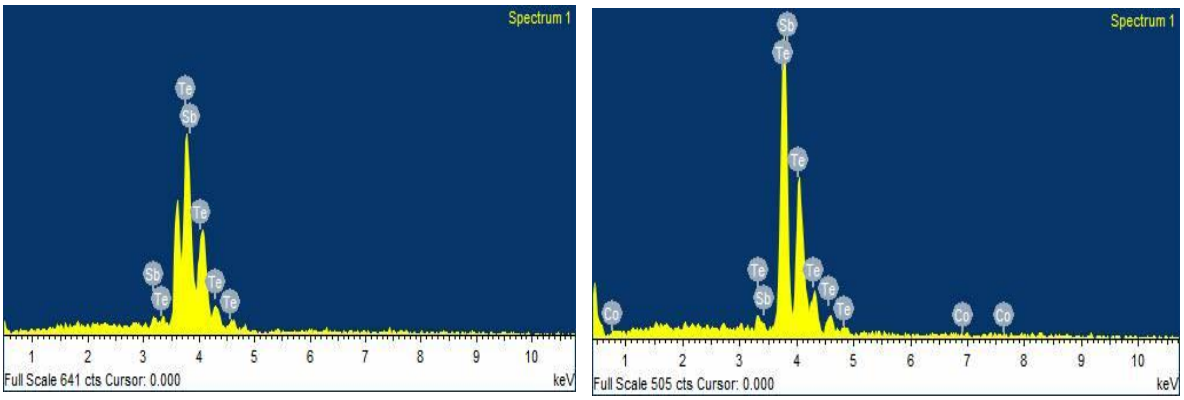

Fig.7.3 (a, b) Represents the EDX spectra of the samples x=0 and x=0.10 respectively.

pure sample (x=0) contains only Sb and Te elements [Fig. 7.3(a)] whereas the doped sample x= 0.10 was showing Sb, Te and Co elements [shown in Fig. 7.3(b)]. On the basis of these experimental results we can conclude that Co have been doped in Sb_2Te_3 lattice without any clustering or precipitation. No extra element such as O or C has been seen in samples indicating that the as prepared samples were excellent in purity and hence ruling out the presence of any impurity in the samples.

Since the surface of TIs are special and different from normal materials so we have characterized the surface of the single crystals of x=0 and x=0.10 samples using SEM and AFM. Fig. 7.4(a, b) display the SEM images of as-prepared product x=0 and 0.10 samples

respectively. The structure of Sb_2Te_3 consist of quintuple layers arranged in Te-Sb-Te-Sb-Te sequence along the c axis having planar, covalently bonded sheets and these quintuple layers are weakly bonded together to form the crystals by weak van der Waals interactions. It can be clearly seen from the SEM images that the as prepared single crystals (x=0 and 0.10) exhibits a layered structure similar to that reported by Li et al. [140]. It is also obvious from the SEM images that the planes are stacked one by one to form the crystals.

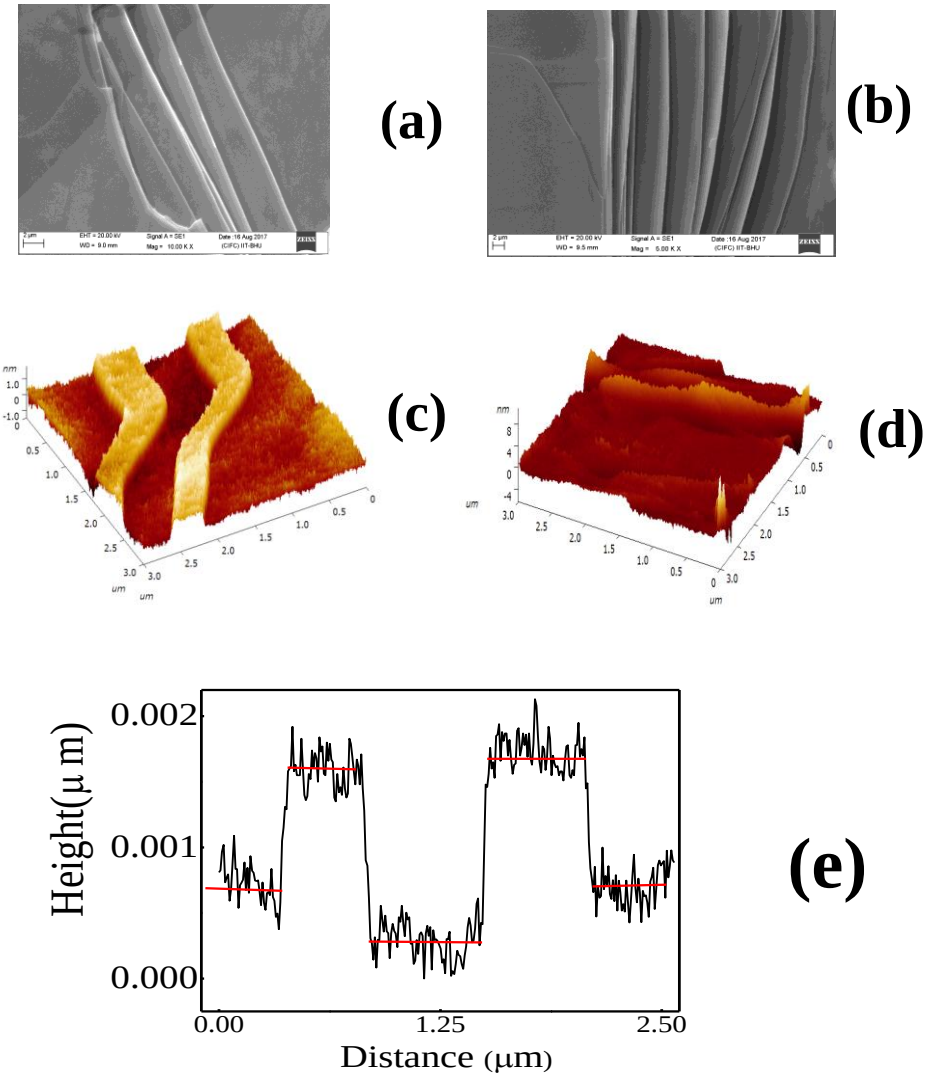

Fig.7.4 (a, b) Show the SEM images of the samples x=0 and x=0.10 respectively. (c, d) Represents the 3D AFM images of x=0 and x=0.10 samples respectively, (e) shows the variation of height vs. scanned distance for x=0 sample.

Since only 2D picture could be seen using SEM images therefore for the 3D images, we have further examined the surface morphology of the single crystals by AFM measurement. Fig. 7.4(c) and (d) are the AFM images of the samples x=0 and x=0.10 respectively. We can easily see the layers present in the single crystals of x=0 samples [Fig. 7.4(c)], but it is not so clear in x=0.10 sample [Fig. 7.4(d)]. The extracted average roughness from AFM analysis was 0.416 nm for x=0 sample, which was increasing with the doping concentration of Co and finally reaches up to 0.731 nm, this fact also support the substituting of Co in Sb_2Te_3 lattice. We have also calculated thickness of the layers from the scanned distance Vs. Height graph [shown in Fig. 7.4(e)] for the sample x=0, the determined average thickness of the layers was 10.3Å which is very close to the thickness of one quintuple having thickness10Å.

7.2.3 XPS Analysis

A typical set of survey and core level spectra were recorded under ultra-high vacuum (UHV) conditions. For survey spectrum the pass energy of the analyser was kept at 187.5 eV whereas for the core level the spectrum was acquired at a low set of pass energy 11.750 eV or 23.6 eV to achieve a better resolution. The binding energies were calibrated with the C1s reference (284.5eV). Fig.7.5 represents the survey spectrum of x=0.10 sample, the peaks corresponding to Sb and Te were prominent in the spectrum while the peaks associated with Co were very weak in intensity, which is due to the low concentration of Co in the sample. High resolution XPS spectrum corresponds to energy region of Co 2p is been shown in the inset of Fig.7.5 (b) for the sample x=0.10. Two main peaks at 778.4eV and 793.4eV have been found corresponding to Co $2p_{3/2}$ and Co $2p_{1/2}$ energy levels respectively. The energy gap between the levels Co $2p_{3/2}$ and Co $2p_{1/2}$ is 15 eV which was very close to the reported

value [141]. Peak associated with 781.8 eV is attributed to Co^{2+} state. Two characteristic satellite peaks on the high energy side of Co $2p_{3/2}$ at the energy around 784.47 eV and 787.97 eV also confirm the presence of Co^{2+} state. Peak around 780.02 eV is associated with the mixed Co^{2+} and Co^{3+} bonding states [142]. Moreover the low intensity of these satellite peaks also indicates about the mixing of Co^{2+} and Co^{3+}states. Besides these factors, the asymmetry in the Co $2p_{1/2}$ peak also confirms the presence of mixed states of both Co^{2+} and Co^{3+} ions [143].

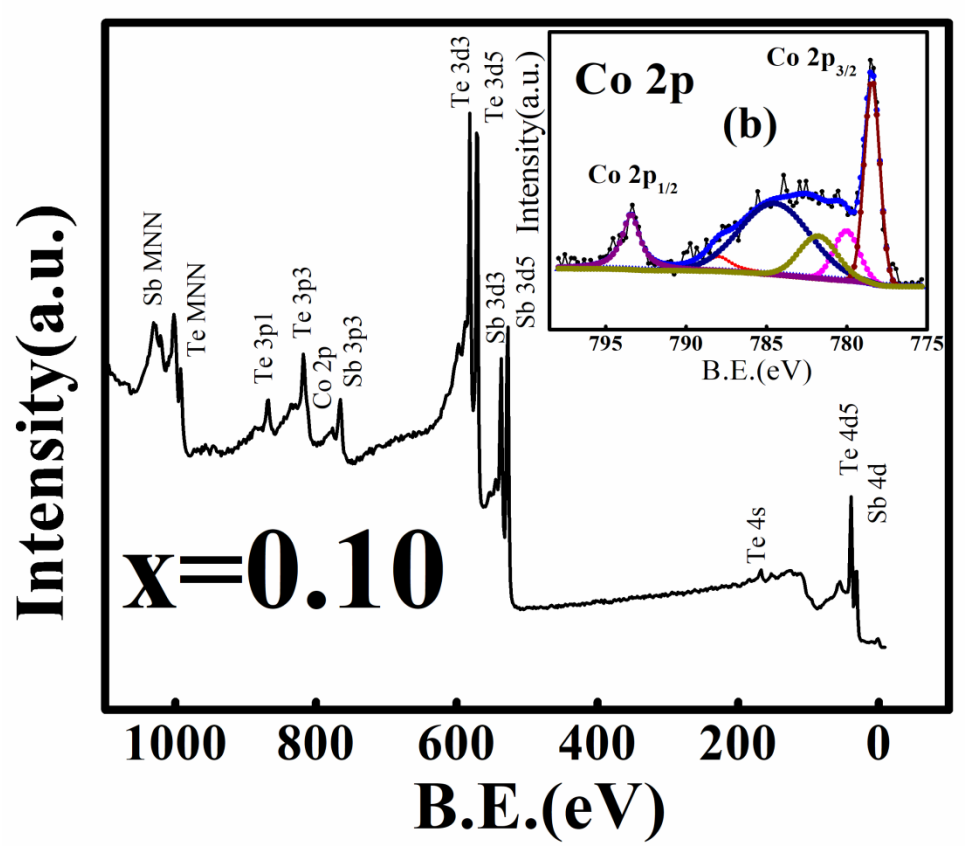

Fig. 7.5 Represents the XPS survey scan of x=0.10 sample, Inset: XPS high resolution core level spectra of Co region (2p).

7.2.4 Study of Magnetic Properties

We have measured magnetization (M) as a function of temperature (T) as well as applied magnetic field (H) of the $Sb_{2-x}Co_xTe_3$ (x=0, 0.02, 0.06, 0.10) samples. M-T measurement has been performed in the temperature range of $2K \leq T \leq 300K$ at the applied field of 1000 Oe in the zero-field cooled (ZFC) mode. Fig. 7.6 shows the magnetization vs. temperature graph for the $Sb_{2-x}Co_xTe_3$ (x=0.02, 0.06, 0.10) samples. The value of magnetization is found to be positive throughout the temperature range $2K \leq T \leq 300K$ for the samples x=0.02 and 0.06 but the scenario is different for x=0.10 sample where the value of magnetization was negative around 10K. M-T curve was clearly indicating that the magnetic state present in x=0.10 sample was different from the magnetic state present in x=0.02 and x=0.06 samples.

For further confirmation of magnetic state, we have carried out magnetization measurement (M) as a function of applied magnetic field (H) at different constant temperatures (*viz*. at 2K, 10K, 50K, 150K, 200K and 300K) under the applied field range of -2T to 2T for all the samples (x=0.02, 0.06 and 0.10) which are shown in Fig. 7.7. Non linearity and hysteresis loop at low field could be observed for both the doped samples x=0.02 and 0.06. No sign of saturation in magnetization is observed up to applied field of 2T, which is an indication of antiferromagnetic state for these samples. Therefore, it is clear from the M (H) curve that the samples are showing antiferromagnetic ordering at lowest temperature 2K and retain antiferromagnetic ordering even at room temperature 300K. Whereas x=0.10 sample was showing diamagnetic behavior in the temperature region above 10K. Moreover as the concentration of Co was increasing from x=0.02 to0.10, area under hysteresis curve was decreasing [shown in Fig. 7.7(d)] but the maximum value of

magnetization was increasing from x=0.02 to x=0.06 at 2T and it decreasing after further doping concentration of Co (x=0.10). The M-H curves for the samples x=0.02, 0.06 and 0.10 at temperatures 2K and 300K are shown in Fig. 7.7 (d). Pure Sb_2Te_3 is well established diamagnetic material. The surface effects are more pronounced in comparison to the corresponding bulk state in these Topological insulators. For the magnetic properties, the influence of uncompensated surface spins on the saturation magnetization plays a crucial role. Therefore, Co may induce the surface-enhanced spin polarization, and even in the absence of magnetic ions, it promotes the

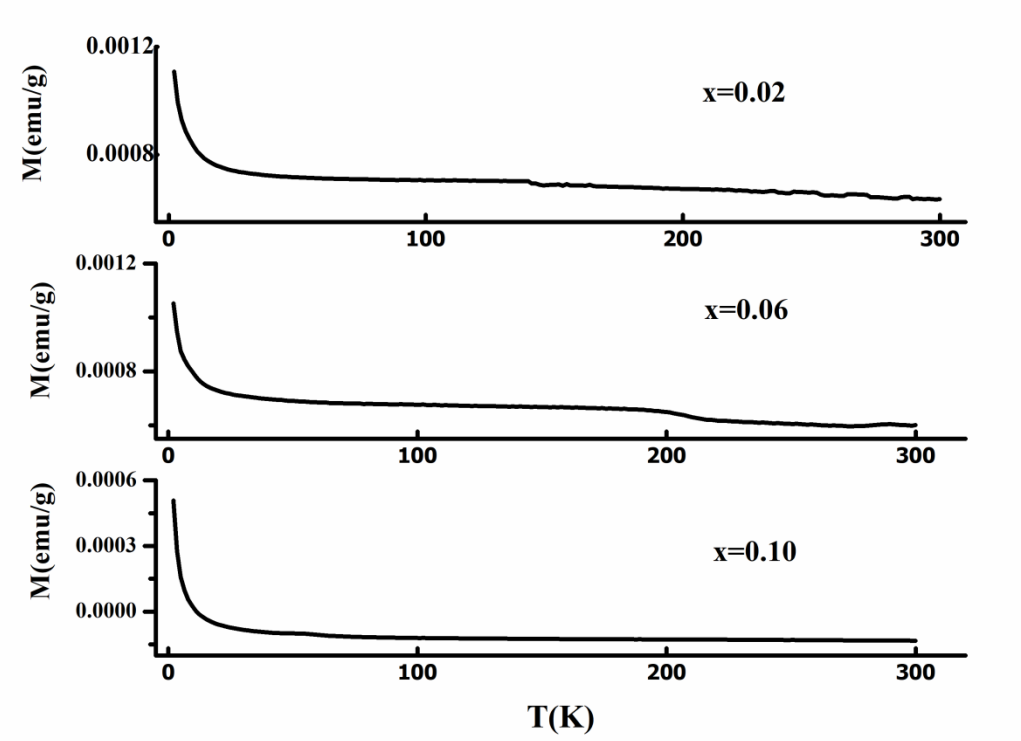

Fig.7.6 Shows the variation of magnetization (M) vs. temperature (T) for the Co doped samples (x= 0.02, 0.06, 0.10).

formation of extended magnetic states, which are missing in the bulk counterpart. In this way, the surface may show uncompensated spins ferromagnetically ordered, even for an

antiferromagnetic alignment of Co spins. It has already been shown that in the doped samples Co exists both in +2 and +3 states. The exchange between these two is antiferromagnetic. As a matter of fact, the co-existence of both ferromagnetic and anti-ferromagnetic states are observed. As we increase temperature, coercive field decreases which might be due to the

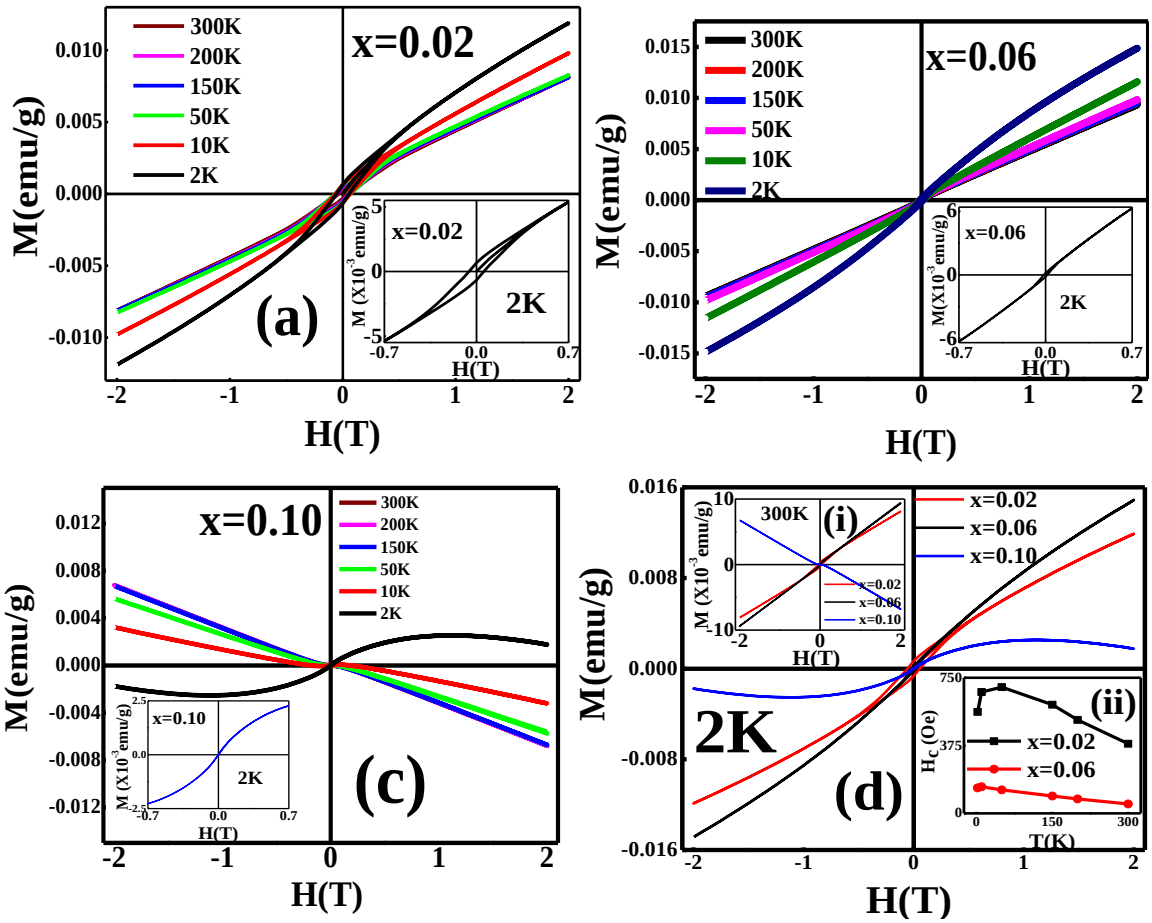

Fig.7.7 (a, b, c) show the variation of magnetization (M) vs. applied field (H) for the Co doped samples (x= 0.02, 0.06, 0.10) respectively. Inset of Fig. 7.7 (a), (b) and (c) represents the zoom picture of MH behavior at 2K. Fig. 7.7 (d) represents compile picture of M vs. H behavior for the samples (x= 0.02, 0.06, 0.10) at 2K, Inset (I): shows the compile picture of M vs. H for the samples (x= 0.02, 0.06, 0.10) at 300K, Inset (II) represents the variation of coeresive field (H_C) as a function of Temperature (T) for the samples x=0.02 and x=0.06.

thermal agitation of spin. As we increase the concentration of Co from x=0.20 to 0.06, ions become nearer to each other and the relative distance between them reduces which gives rise to repulsive force and due to which antiparallel arrangement becomes more favorable between the spins and hence spins started to become antiparallel, and due to the

superexchange interaction between Co^{2+} and Co^{3+}, area of hysteresis reduces for the higher concentration of Co. But as we increase the Co concentration from x=0.02 to x=0.06, more number of spins orient itself in the direction of field with the increase of the applied field and higher magnetization results [shown in Fig. 7.7(d)]. Furthermore at Co concentration up to x=0.10, distance between the spins decreases and hence superexchange interaction increases and as a result there is enhancement of antiferromagnetic ordering in exchange of ferromagnetic ordering. As a matter of fact, weak antiferromagnetization with diamagnetic background has been observed which might be due to parent Sb_2Te_3. In fact, this is well known that the low energy physics for a three dimensional topological insulator can be described by the spin-momentum locking. The helicity of the spin texture is left handed for the upper Dirac cone and right handed for the lower Dirac cone. The point where the two bands of opposite helicity meet each other, i.e. at the Dirac node, the spins are free to align along the direction of the external magnetic field. This intrinsic paramagnetic contribution to the magnetic moment of the system is observed in the M (H) curve for the x=0.10 sample.

7.3 Conclusion

Room temperature antiferromagnetic ordering has been found in Co doped Sb_2Te_3 while the parent material Sb_2Te_3 is diamagnetic in nature. This may be due to the mixed valence state of Co^{2+} and Co^{3+} ions confirmed by the XPS analysis. By developing such type of magnetic TIs, showing magnetic ordering at RT, a new way may open to design and develop future spintronics and electronic devices which may be important in quantum computing and multifunctional electromagnetic applications.